# Atomically Precise Growth of Catalytically Active Cobalt Sulfide on Flat Surfaces and within a Metal−Organic Framework *via* Atomic Layer Deposition

Aaron W. Peters,[†] Zhanyong Li,[†] Omar K. Farha,[*,†,‡] and Joseph T. Hupp[*,†]

[†]Department of Chemistry, Northwestern University, 2145 Sheridan Road, Evanston, Illinois 60208, United States and [‡]Department of Chemistry, Faculty of Science, King Abdulaziz University, Jeddah 22254, Saudi Arabia

ABSTRACT Atomic layer deposition (ALD) has been employed as a new synthetic route to thin films of cobalt sulfide on silicon and fluorine-doped tin oxide platforms. The self-limiting nature of the stepwise synthesis is established through growth rate studies at different pulse times and temperatures. Additionally, characterization of the materials by X-ray diffraction and X-ray photoelectron spectroscopy indicates that the crystalline phase of these films has the composition Co_9S_8. The nodes of the metal−organic framework (MOF) NU-1000 were then selectively functionalized with cobalt sulfide *via* ALD in MOFs (AIM). Spectroscopic techniques confirm uniform deposition of cobalt sulfide throughout the crystallites, with no loss in crystallinity or porosity. The resulting material, CoS-AIM, is catalytically active for selective hydrogenation of *m*-nitrophenol to *m*-aminophenol, and outperforms the analogous oxide AIM material (CoO-AIM) as well as an amorphous CoS_x reference material. These results reveal AIM to be an effective method of incorporating high surface area and catalytically active cobalt sulfide in metal−organic frameworks.
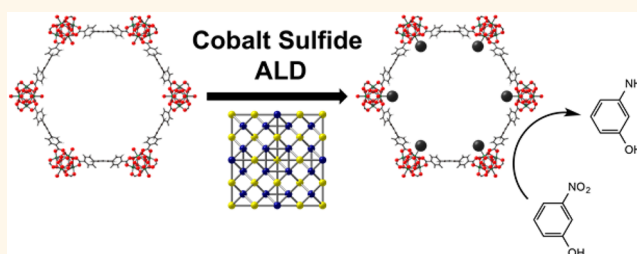
KEYWORDS: atomic layer deposition · nanoscale Co_9S_8 films · metal−organic framework

Nanostructuring of transition metal sulfides (TMS) has tremendously improved the activity of hydrodesulfurization[1,2] and proton reduction[3,4] catalytic processes. In addition to an increased exposed surface to volume ratio, nanostructured materials may differ both structurally and electronically from corresponding bulk versions of the materials.[5,6] For example, detailed mechanistic and theoretical studies have indicated that the edge sites of nanoparticulate MoS_2 have an increased density of catalytically active under-coordinated Mo and S atoms.[7,8] Therefore, the fabrication of nanostructured TMS with precise surface morphologies and sizes is an important area of research. Current methods to nanostructure TMS include hydrothermal, solvothermal, and templated growth.[9−11] These routes often involve high temperatures, condensed-phase reaction media, and multiple synthetic steps, that may impede the synthesis of nanostructured TMS with well-defined and uniform morphologies and sizes.[12−14]

One possible method to construct TMS with precise surface structuring is atomic layer deposition (ALD), a vapor-phase deposition technique capable of yielding high purity, conformal films of inorganic compounds with subnanometer control over film thickness.[15,16] In contrast to chemical vapor deposition (CVD), a line-of-sight synthesis technique, ALD is characterized by inherently self-limiting synthesis cycles, *i.e.*, complete and irreversible reactions that saturate the surface of the supporting material, even if the support is porous or presents a complex geometry. Because of the sequential and self-limiting nature of the ALD process, films with unique morphologies can be grown in

essentially layer-by-layer fashion.[17−19] Thus far, ALD research has largely focused on the growth of metals and oxides, whereas TMS have been less studied, despite the important potential applications for these materials. In particular, cobalt sulfide, which has potential electrochemical, photonic, and catalytic applications, is not among the 16 binary TMS materials grown *via* ALD in the literature.[20] Of the many crystalline phases of cobalt sulfide (*e.g.*, CoS, CoS_2, Co_3S_4), Co_9S_8 is most notable for its use in hydrodesulfurization reactions,[21] hydrogen evolution,[22] oxygen reduction,[23] and as a supercapacitor.[24] Unfortunately, the synthesis of Co_9S_8 often involves high temperatures (>400 °C), and multiple steps.[21,24] Moreover, it readily oxidizes to form cobalt oxide impurities if syntheses are conducted in environments that are not stringently free of oxygen.[25−27] Well-defined, catalytically active, and high surface area bulk powders and thin films of Co_9S_8 are therefore laborious to fabricate. Herein, we describe a simple method for growing thin films of Co_9S_8 *via* vapor-phase ALD using commercially available precursors; bis(*N,N′*-di-*i*-propylacetamidinato)cobalt(II) (Co(amd)$_2$) (Figure 1) and H_2S.

To take advantage of this new route to cobalt sulfide in a catalytic system, we turn to metal−organic frameworks (MOFs) as a scaffold. MOFs are crystalline, high surface area,[28] and porous materials composed of inorganic metal clusters or ions and organic linkers that have potential applications in catalysis,[29−31] gas storage and separations,[32−34] and light harvesting.[35] In an effort to generate highly disperse and high surface area catalysts, metals and metal oxides have been successfully incorporated in MOFs *via* condensed phase routes (*e.g.*, transmetalation[36,37] or impregnation[38,39]) yielding highly active heterogeneous catalysts.[40] Methods to anchor catalytically active TMS to MOFs, however, are generally lacking, presumably due to the instability of many MOFs toward the common sulfur source, H_2S.[41−43] Current routes to incorporate TMS in MOFs either involve nanoparticle or quantum dot deposition from non-hydrogen sulfide precursors[44,45] or complete decomposition of the MOF to form TMS carbon composites.[46−48] Recently, we described the installation of zinc(II) and aluminum(III) on the hexa-zirconium(IV)aqua/hydroxo/oxo nodes of the mesoporous MOF, **NU-1000** *via* AIM (ALD in MOFs).[38] We extend this work to sulfides by using the ALD
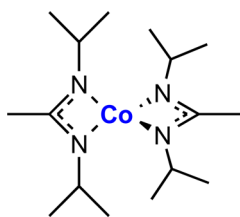
deposition of cobalt sulfide into **NU-1000** to form a highly stable cobalt sulfide functionalized MOF, **CoS-AIM**. To our knowledge, no deposition technique involving the selective incorporation of TMS on the nodes of MOFs with or without using H_2S as a sulfur source has been reported. In a proof-of-principle type reaction, we tested the ability of the CoS_x sites in **CoS-AIM** to catalyze the condensed-phase hydrogenation of *m*-nitrobenzene to *m*-aminobenzene using sodium borohydride. The material was found to display excellent catalytic activity and recyclability.

RESULTS AND DISCUSSION

ALD of Co_9S_8 Films on Silicon and FTO. Cobalt sulfide films were grown at 130 °C on both silicon and fluorine-doped tin oxide (FTO) supports. Alternating doses of Co(amd)$_2$ and H_2S were pulsed using the timing sequence of $t_1−t_2−t_3−t_4$ (all times in s): corresponding to pulse time of Co(amd)$_2$, the purge time after the cobalt pulse, the pulse time of H_2S, and the subsequent purge time after the H_2S pulse, respectively. The self-limiting nature of Co(amd)$_2$/H_2S reactivity was established by varying the pulse times of the two precursors and measuring the thickness of the films grown on silicon *ex situ* using optical ellipsometry (Figure 2a,b). Plateaus in growth occurred at 1 s for Co(amd)$_2$ and 0.015 s for H_2S and subsequent tests were conducted with the timing sequence 1−20−0.015−20 s. Growth rates were measured as a function of temperature from 130 to 225 °C and were observed to remain constant at *ca.* 0.4 Å/cyc (Figure S1 in the Supporting Information), indicating no thermal decomposition of the precursors, as expected for an ALD process. (CVD growth rates usually have a stronger dependence on substrate
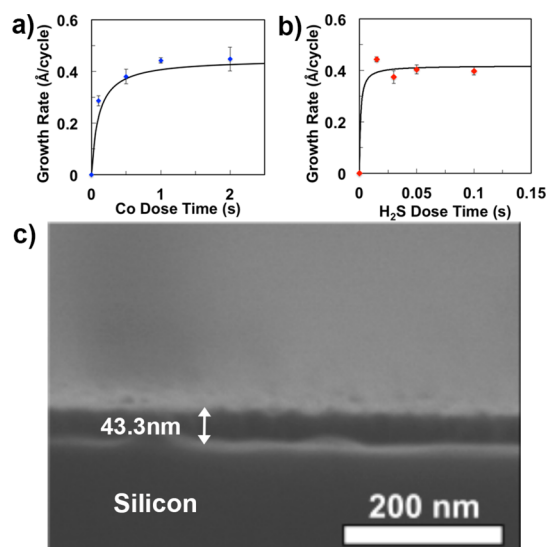
Figure 2. Growth characteristics of ALD cobalt sulfide films. (a) Growth rate *versus* cobalt precursor pulse time at a deposition temperature of 130 °C. **(b)** Growth rate *versus* H_2S pulse time at a deposition temperature of 130 °C. **(c)** SEM image of a 1000 AB cycle film of Co_9S_8 on silicon.

Figure 1. Structure of the cobalt precursor, bis(*N,N′*-di-*i*-propylacetamidinato)cobalt(II).

temperature.)[15] Scanning electron microscopy (SEM) (Figure 2c) was used to image a 1000 AB cycle film and its thickness was determined to be *ca.* 43 nm, which agrees well with the 0.4 Å/cyc growth rate measured *via* ellipsometry.

The crystalline phase of these films was determined to be Co_9S_8, based on the X-ray diffraction (XRD) pattern of an as-deposited film consisting of 1000 AB cycles of $Co(amd)_2$ and H_2S on silicon (Figure 3a). Raman spectroscopy (Figure 3b) performed on Co_9S_8 films grown on FTO exhibits sharp peaks at 691, 520, and 481 cm^{-1} in excellent agreement with other reported Co_9S_8 materials.[22] The films were further characterized using
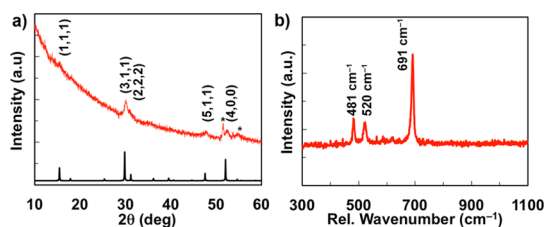

Figure 3. Characterization of Co_9S_8 films. (a) XRD pattern of a 1000 cycle Co_9S_8 film on Si (top) and simulated pattern of Co_9S_8 (bottom). Asterisks (*) indicate peaks from silicon material. (b) Raman spectrum of 1000 AB cycle Co_9S_8 film grown on FTO.
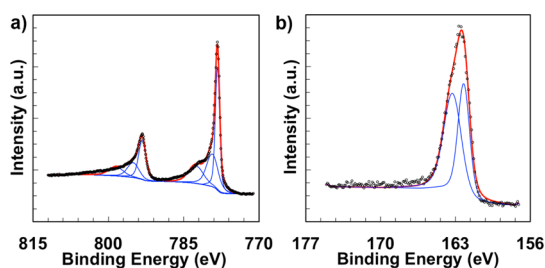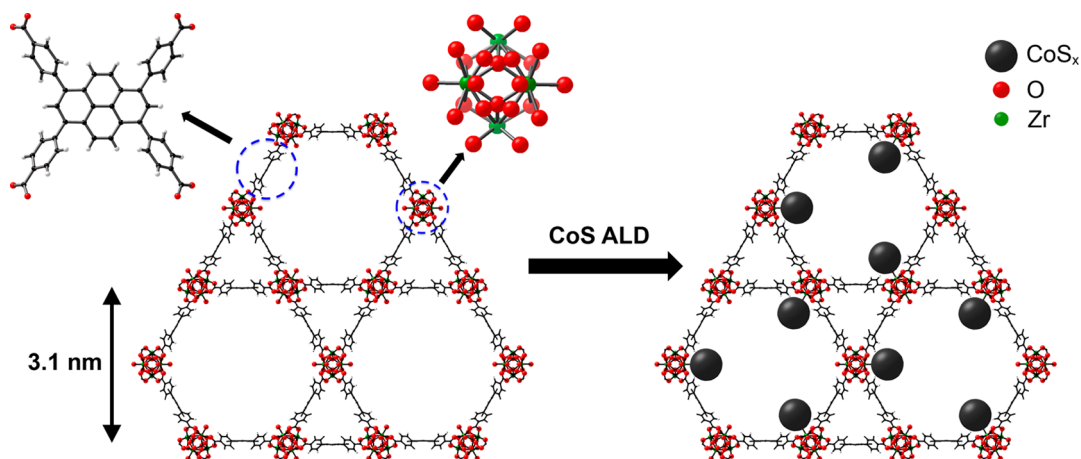

Figure 4. XPS spectra for as grown Co_9S_8 films on silicon (a) Co 2p region, (b) S 2s region. Black circles indicate raw data; blue and red lines indicate peak and cumulative fit, respectively.

X-ray photoelectron spectroscopy (XPS) as shown in Figure 4. Features at 778.3, 779.3, and 782.6 eV are attributed to the cobalt $2p_{3/2}$ peaks, which agree well with literature reported values for Co_9S_8.[49,50] The peak at 162.2 eV most likely corresponds to an unresolved doublet of the 2p shell of S^{2-}. Films that were purposely exposed to ambient conditions experienced oxidation of both the Co and S species as indicated by the XPS spectra (Figure S2), which showed an appearance of a peak at 166.3 eV corresponding to S^{6+}, and a concomitant disappearance of the Co^0 $2p_{3/2}$ at 778.3 eV, presumably due to the oxidation of Co^0 to Co^{2+}. Finally, quantitative energy—dispersive X-ray spectroscopy (EDS) suggests a Co:S ratio of 51:49, providing further evidence for the assignment of the phase as Co_9S_8 (Figure S3).

Atomic Layer Deposition of Cobalt Sulfide in a Metal—Organic Framework. After confirming ALD growth behavior of cobalt sulfide with $Co(amd)_2$ and H_2S on flat surfaces, we next sought to investigate cobalt sulfide deposition in the MOF **NU-1000** with the goal of producing highly dispersed, thereby more catalytically active, cobalt sulfide material. **NU-1000**, in this case, was selected as the MOF platform due to its excellent chemical and thermal stability as well as its precedented successful elaboration by ALD. **NU-1000** is composed of $Zr_6(\mu_3-O)_4(\mu_3-OH)_4(H_2O)_4(OH)_4$ nodes and tetratopic 1,3,6,8-(*p*-benzoate)pyrene (H_4TBAPy) linkers which form large 3.1 nm wide mesoporous hexagonal channels. The channels are addressable *via* ALD in a similar fashion to the flat surfaces due to reactive terminal hydroxyl and aqua ligands on the Zr_6 nodes that are orientated toward the center of the pores as depicted in Scheme 1. In principle, we can develop nanostructured cobalt sulfide materials with enhanced catalytic performance as compared to bulk counterpart analogues due to site isolation and increased surface area of the deposited material *via* conducting ALD in **NU-1000**.

Scheme 1. Representative structure of NU-1000. Circles highlight the Zr_6 node and the pyrene linker. ALD of 1 AB cycle of cobalt sulfide produces cobalt sulfide functionalized NU-1000 with approximately one CoS_x site per Zr_6 node.

We assessed the stability of **NU-1000** to H$_2$S first by exposing the MOF to a stream of 1% H$_2$S at 130 °C for 1 h. Powder X-ray diffraction (PXRD) patterns of the pre- and postexposure samples show no discernible change, indicating that **NU-1000** remains crystalline (Figure S4). N$_2$ adsorption-desorption isotherms measured at 77 K of the MOF after H$_2$S exposure are essentially identical to that of the parent material (Figure S5), indicating that neither porosity nor internal surface area is diminished. These findings regarding hydrogen sulfide exposure stand in striking contrast to those reported for various other MOFs.[41−43,51] Encouraged by these results, we set out to functionalize **NU-1000** with cobalt sulfide *via* an ALD-like process similar to that of the procedure discussed earlier. One major challenge of AIM is the relatively slow diffusion of the precursors through the material. However, due to the presence of the mesopores in NU-1000, this can be easily addressed by using additional exposure time for the deposition. Therefore, a timing sequence of 1−240−0.015−120 s was used for this process, corresponding to the pulse time of Co(amd)$_2$, exposure time of the cobalt precursor, pulse time of H$_2$S, and the exposure time of H$_2$S, respectively. Each precursor was dosed multiple times before advancing to the second precursor to ensure complete saturation of each reactant under the experimental conditions.

To measure the cobalt and sulfur content in the synthesized material, **NU-1000** with 1 AB cycle of cobalt sulfide growth (denoted hereafter as **CoS-AIM**) was digested and analyzed by inductively coupled plasma−atomic emission spectroscopy (ICP−AES) to determine that, on average, 1.2 cobalt and 1.1 sulfur is present on each Zr$_6$ node. Nitrogen adsorption-desorption isotherms measured at 77 K (Figure 5a) indicate a decrease of Brunauer−Emmett−Teller (BET) surface area from 2170 to 1650 m^2/g, which is consistent with our previously reported AIM materials.[38] To assess the uniformity of deposition of Co and S in NU-1000, EDS line-scans were measured across a single crystallite of **CoS-AIM** and no concentration gradient was observed for either element (Figure 5b,c). XPS results verify the presence of Co^{2+} and S$^{2−}$ as would be expected for a cobalt sulfide cluster; however, the broadness of the peaks in XPS spectra (Figure S7) imply that the cobalt sulfide is an amorphous phase. Importantly, the PXRD pattern of the **CoS-AIM** material confirms that the MOF maintains its crystallinity after cobalt sulfide functionalization (Figure 6).

To elucidate the chemical nature of the growth sites for the CoS$_x$ species, diffuse reflectance infrared Fourier transform spectroscopy (DRIFTS) was used to monitor changes in the O−H stretching region, as the unreacted Zr$_6$ nodes are known to consist of both aqua and hydoxo ligands.[52] A sample of **CoS-AIM** with higher cobalt loading was synthesized in order to more easily observe changes in these stretches upon
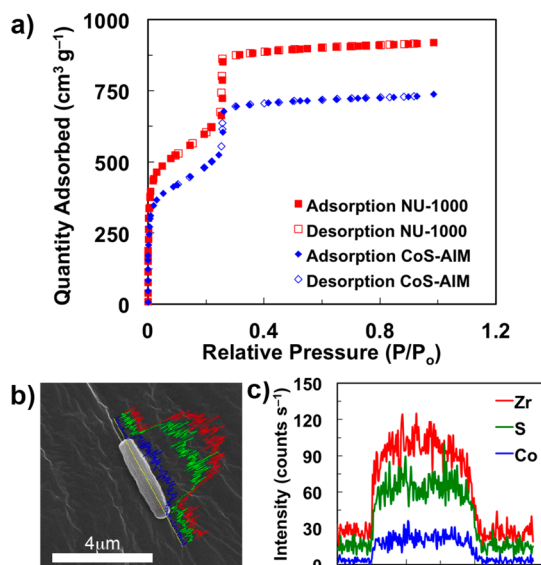
Figure 5. Characterization of CoS-AIM. (a) N$_2$ adsorption-desorption isotherms of NU-1000 before and after cobalt sulfide ALD. (b) SEM image of CoS-AIM. (c) Corresponding EDS line scans of CoS-AIM showing uniform incorporation of Co and S throughout a single crystallite.
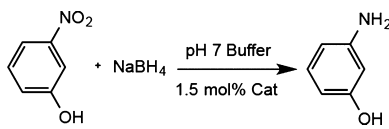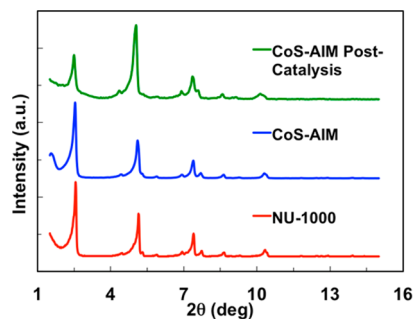
Figure 6. PXRD patterns for NU-1000, CoS-AIM, and CoS-AIM after hydrogenation of *m*-nitrophenol.

anchoring CoS$_x$. This sample was prepared by increasing the number of cobalt pulses and the exposure time to 300 s for Co(amd)$_2$. ICP−AES analysis of this sample reveals a Co/Zr$_6$ ratio of 7.5, which suggests near saturation of the nodes such that all available grafting sites (−OH, −OH$_2$) should be occupied. Accordingly, the IR spectrum (Figure S9) of this material shows a significant decrease in intensity of the peak at 3674 cm^{-1}, assigned to terminal −OH groups, as well as a decrease or complete loss of the signals at 2745 and 2551 cm^{-1}, which are ascribed to the hydrogen-bonded aqua ligands on the node.[52] These data seem to verify the hypothesis that cobalt sulfide growth occurs initially *via* reaction with the hydroxide and aqua ligands of the Zr$_6$ node. Additionally, DFT pore-size distributions (Figure S10) calculated from N$_2$ isotherms signify a small decrease in pore size from 30 to 27 Å implying growth of cobalt sulfide within the hexagonal channels.

Catalysis of Nitroaromatics to Amines Using CoS-AIM. With the **CoS-AIM** material in hand, we were interested in

TABLE 1. Reduction of *m*-Nitrophenol

catalyst[a]	conversion (%)
NU-1000	0
Co$_9$S$_8$ Films	0
CoO-AIM	1
CoS$_x$	70 (30)[b]
CoS-AIM	99

[a] Conditions: 1.5 mol % catalyst based on CoS$_x$ content, 20 mg *m*-nitrophenol, 200 mg of NaBH$_4$, and 8 mL of 1.0 M, pH 7, tris(hydroxymethyl)aminomethane buffer. Conversion % is determined from ^{1}H NMR. [b] Conversion based on total conversion to all hydrogenated products. Parentheses indicate conversion to desired *m*-aminophenol product.

investigating its catalytic activity for the selective hydrogenation of nitroaromatic compounds to amines, a common test reaction for gauging the effectiveness of metal hydrogenation catalysts (including various cobalt sulfides).[53−55] The reduction of *m*-nitrophenol to *m*-aminophenol (Table 1) was studied in a 1.0 M, pH 7 tris(hydroxymethyl)aminomethane buffer solution using 1.5 mol % **CoS-AIM** (based on CoS$_x$) with sodium borohydride as a hydrogen source.[56] An amorphous CoS$_x$ material (Co:S ratio calculated to be 0.87 from ICP−AES data), used previously to hydrogenate nitro-aromatics, was solvothermally synthesized according to a literature procedure to serve as a reference material.[57] Under these conditions, **CoS-AIM** completely converts *m*-nitrophenol to *m*-aminophenol (determined from ^{1}H NMR spectroscopy after workup) after 15 min. For comparison, under identical catalyst loadings and reaction conditions, the reference material yielded incomplete hydrogenation in addition to the formation of a mixture of undesired products such as azobenzene and azoxybenzene derivatives attributed to slower kinetics as seen in other hydrogenation catalytsts.[54] High catalytic activity in **CoS-AIM** can be credited to the higher surface area of the MOF (1650 m^2/g) compared to the reference material (40 m^2/g), yielding additional active sites in the MOF sample. Films of ALD-grown Co$_9$S$_8$ on silicon were likewise tested for hydrogenation and showed no catalytic activity, presumably due to low number of exposed active sites from the conformal

and pinhole-free films. Also examined was a cobalt oxide/hydroxide functionalized version of **NU-1000**. This material was synthesized similarly to **CoS-AIM** but with water replacing H$_2$S in the B part of the AB AIM cycle. With identical cobalt loading to that in the **CoS-AIM** experiments, **CoO-AIM** converted less than *ca.* 1% of the nitrobenzene after 15 min, underscoring the importance of sulfur (sulfide) in engendering catalytic activity (Figure S15).

To assess the recyclability of **CoS-AIM**, the catalyst was recovered by centrifugation, washed with water and ethanol, and reused for the hydrogenation reaction. Complete conversion of the reactant to *m*-aminobenzene was observed even after three runs (Figure S16). The PXRD pattern of **CoS-AIM** after catalysis indicates that the crystallinity of the hybrid MOF material is retained (Figure 6). ICP−AES analyses show that ratios of cobalt to sulfur and to zirconium are unaffected by the material's use as a catalyst, implying that AIM-installed CoS$_x$ does not leach from the MOF. SEM−EDS line scans show that cobalt and sulfur remain uniformly distributed through the crystallite (Figure S17). These data together suggest that **CoS-AIM** is a robust and effective heterogeneous hydrogenation catalyst.

CONCLUSIONS

In summary, we have developed a technique to deposit films of cobalt sulfide with subnanometer level precision on silicon and FTO substrates using ALD. This technique was also employed to functionalize the nodes of the MOF **NU-1000** with cobalt sulfide (**CoS-AIM**). Impressively, the CoS$_x$ sites in **CoS-AIM** catalytically hydrogenate *m*-nitrophenol to *m*-aminophenol more rapidly than does the cobalt oxide analogue or a CoS$_x$ reference material, a testament to the highly dispersed nature of the nanostructured CoS$_x$ sites in the **CoS-AIM** material. These results demonstrate another tool available for post-synthesis modification of MOFs, specifically access to metal sulfides, an under-utilized class of catalytic materials in the MOF literature. Owing to the abundance of available transition metal ALD precursors, we believe that the technique described here can be used to incorporate many other nanostructured transition metal sulfide materials in MOFs for potential applications in other catalytic processes such as hydrogen evolution and hydro-desulfurization.

METHODS

Chemicals. Bis(*N*,*N*′-di-*i*-propylacetamidinato)cobalt(II) (98%) was purchased from Strem Chemicals, Inc. A solution of 1% H$_2$S in N$_2$ was obtained from Matheson Tri-Gas. ZrOCl$_2$·8H$_2$O (98%), benzoic acid (>99.5%), CoCl$_2$·6H$_2$O (98%), thiourea (99%), tris(hydroxymethyl)aminomethane (99.8%), NaBH$_4$ (98%), and 3-nitrophenol (99%) were obtained from Sigma-Aldrich. The chemicals used in the synthesis of H$_4$TBAPy were the same as

our previous report. Dimethylformamide (DMF, 99.8%) and ethyl acetate (99.5%) were obtained from Macron Fine Chemicals. Acetonitrile-*d$_3$* (99.8%) was purchased from Alfa Aesar. All chemicals were used without further purification.

Co$_9$S$_8$ ALD. Silicon wafers and FTO were cut into *ca.* 1.5 × 1.5 cm^2 squares and cleaned by sonicating in a bath of soapy water, deionized water, isopropyl alcohol, and acetone for 15 min each. ALD was carried out on a Savannah 100

(Cambridge Nanotech, Inc.). The cobalt precursor was heated to 120 °C, and the silicon and FTO surfaces were heated to 130 °C unless noted otherwise. The timing sequence 1−25−0.015−25 s was used for Co(amd)$_2$ and H$_2$S for most studies. Cobalt sulfide materials were characterized using scanning electron microscopy (SEM, SU8030, Hitachi), ellipsometry (J.A. Woollam M2000U), X-ray photoelectron spectroscopy (XPS, ESCALAB 250Xi, Thermo Scientific). The crystal structure was determined using grazing−incidence X-ray diffraction (GIXRD, ATX-G, Rigaku) and confocal Raman spectroscopy (TriVista CRS, Princeton Instruments).

Preparation of CoS-AIM. NU-1000 was synthesized and activated according to a modified literature procedure. In short, ZrOCl$_2$·8H$_2$O (388 mg, 1.20 mmol) and benzoic acid (10.8 g, 88.4 mmol) were added to a 100 mL screw cap jar with 32 mL of DMF. The suspension was dissolved by sonication and subsequently incubated in an 80 °C oven for 1 h. After cooling to room temperature, H$_4$TBAPy (160 mg, 0.24 mmol) was added and the yellow suspension was sonicated for 20 min, then placed in an 100 °C oven for 16 h. Yellow microcrystalline powder was isolated *via* centrifugation and washed with DMF. The activation procedure was conducted according to the literature protocol.[38] For **CoS-AIM**, approximately 30 mg of activated **NU-1000** was placed in a custom-made ALD powder sample holder. The sample was allowed to equilibrate for 30 min in the ALD sample chamber at 130 °C with 15 sccm N$_2$ flow. The following timing sequence was used for cobalt sulfide deposition: 1−240−0.015−120 s. Cobalt pulses were repeated 60 times and H$_2$S was pulsed 40 times to ensure that saturation of each cycle occurred before moving onto the next precursor. **CoO-AIM** was prepared similarly using deionized H$_2$O as the second precursor instead of H$_2$S. **CoS-AIM** with higher loading was prepared using the timing sequence 1−300−0.015−120 s and decreasing the N$_2$ flow to 5 sccm. Cobalt was pulsed 80 times before moving to 60 H$_2$S pulses. Atomic ratios were measured using inductive coupled plasma−atomic emission spectroscopy (ICP−AES, iCAP 7600, Thermo Scientific) by digesting *ca.* 1 mg of the MOF in a nitric acid (1 mL) and 30% H$_2$O$_2$ mixture (0.33 mL) followed by microwave irradiation at 150 °C for 5 min. N$_2$ adsorption-desorption isotherms were collected using a Tristar II 3020 (Micromeritics) at 77 K. DFT pore-size distributions were calculated from N$_2$ isotherms using a carbon slit pore model with an N$_2$ DFT kernel.

Hydrogenation of m-Nitrophenol. The catalyst (1.5 mol % based on Co content), excess NaBH$_4$ (200 mg, 5.3 mmol), and *m*-nitrophenol (20 mg, 0.14 mmol) were added to 8 mL of a 1.0 M, pH 7 tris(hydroxymethyl)aminomethane buffer. Catalytic tests involving Co$_9$S$_8$ films were conducted using a 1 cm^2 square film of 1000 AB cycles (44 nm) Co$_9$S$_8$ deposited on silicon. The reaction mixture was stirred for 15 min and then subsequently centrifuged to isolate the catalyst. The product was extracted using 3 × 10 mL of ethyl acetate. The organic layers were combined and the solvent was removed by a rotary evaporator. The product was dissolved in CD$_3$CN-d_3 for ^{1}H NMR measurements (Avance III 500 MHz, Bruker). After each catalytic run, the catalyst was recovered by centrifugation and further washed in 8 mL of deionized water (×3), 8 mL of ethanol (×3) and dried using a vacuum oven at 60 °C.

REFERENCES AND NOTES

1. Dhas, N. A.; Suslick, K. S. Sonochemical Preparation of Hollow Nanospheres and Hollow Nanocrystals. *J. Am. Chem. Soc.* **2005**, *127*, 2368.
2. Nogueira, A.; Znaiguia, R.; Uzio, D.; Afanasiev, P.; Berhault, G. Curved Nanostructures of Unsupported and Al$_2$O$_3$-supported MoS$_2$ catalysts: Synthesis and HDS Catalytic Properties. *Appl. Catal., A* **2012**, *429−430*, 92.
3. Morales-Guio, C. G.; Stern, L.-A.; Hu, X. Nanostructured Hydrotreating Catalysts for Electrochemical Hydrogen Evolution. *Chem. Soc. Rev.* **2014**, *43*, 6555.
4. Seo, B.; Jung, G. Y.; Sa, Y. J.; Jeong, H. Y.; Cheon, J. Y.; Lee, J. H.; Kim, H. Y.; Kim, J. C.; Shin, H. S.; Kwak, S. K.; *et al.* Monolayer-Precision Synthesis of Molybdenum Sulfide Nanoparticles and Their Nanoscale Size Effects in the Hydrogen Evolution Reaction. *ACS Nano* **2015**, *9*, 3728.
5. Koper, M. T. M. Structure Sensitivity and Nanoscale Effects in Electrocatalysis. *Nanoscale* **2011**, *3*, 2054.
6. Van Santen, R. A. Complementary Structure Sensitive and Insensitive Catalytic Relationships. *Acc. Chem. Res.* **2009**, *42*, 57.
7. Lauritsen, J. V.; Kibsgaard, J.; Helveg, S.; Topsoe, H.; Clausen, B. S.; Laegsgaard, E.; Besenbacher, F. Size-dependent structure of MoS$_2$ nanocrystals. *Nat. Nanotechnol.* **2007**, *2*, 53.
8. Byskov, L. S.; Nørskov, J. K.; Clausen, B. S.; Topsøe, H. DFT Calculations of Unpromoted and Promoted MoS$_2$-Based Hydrodesulfurization Catalysts. *J. Catal.* **1999**, *187*, 109.
9. Gao, M.-R.; Xu, Y.-F.; Jiang, J.; Yu, S.-H. Nanostructured Metal Chalcogenides: Synthesis, Modification, and Applications in Energy Conversion and Storage Devices. *Chem. Soc. Rev.* **2013**, *42*, 2986.
10. Lai, C.-H.; Lu, M.-Y.; Chen, L.-J. Metal Sulfide Nanostructures: Synthesis, Properties and Applications in Energy Conversion and Storage. *J. Mater. Chem.* **2012**, *22*, 19.
11. Zhu, Y.-J.; Chen, F. Microwave-Assisted Preparation of Inorganic Nanostructures in Liquid Phase. *Chem. Rev.* **2014**, *114*, 6462.
12. Lee, Y.-H.; Yu, L.; Wang, H.; Fang, W.; Ling, X.; Shi, Y.; Lin, C.-T.; Huang, J.-K.; Chang, M.-T.; Chang, C.-S.; *et al.* Synthesis and Transfer of Single-Layer Transition Metal Disulfides on Diverse Surfaces. *Nano Lett.* **2013**, *13*, 1852.
13. Lu, Q.; Hu, J.; Tang, K.; Qian, Y.; Liu, X.; Zhou, G. A Simple Method for the Preparation of Nanocrystalline Transition Metal Sulfides. *J. Solid State Chem.* **1999**, *146*, 484.
14. Quintana-Melgoza, J.; Alonso-Nuñez, G.; Homero-Galván, D.; Ávalos-Borja, M. Comparative Activity of Ni−W and Co−Mo Sulfides Using Transition Metal Oxides as Precursors in HDS Reaction of DBT. *Catal. Lett.* **2012**, *142*, 1082.
15. Miikkulainen, V.; Leskelä, M.; Ritala, M.; Puurunen, R. L. Crystallinity of Inorganic Films Grown by Atomic Layer Deposition: Overview and General Trends. *J. Appl. Phys.* **2013**, *113*, 021301.
16. George, S. M. Atomic Layer Deposition: An Overview. *Chem. Rev.* **2010**, *110*, 111.
17. Cleveland, E. R.; Banerjee, P.; Perez, I.; Lee, S. B.; Rubloff, G. W. Profile Evolution for Conformal Atomic Layer Deposition over Nanotopography. *ACS Nano* **2010**, *4*, 4637.
18. Knez, M.; Nielsch, K.; Niinistö, L. Synthesis and Surface Engineering of Complex Nanostructures by Atomic Layer Deposition. *Adv. Mater.* **2007**, *19*, 3425.
19. Williams, V. O.; DeMarco, E. J.; Katz, M. J.; Libera, J. A.; Riha, S. C.; Kim, D. W.; Avila, J. R.; Martinson, A. B. F.; Elam, J. W.; Pellin, M. J.; *et al.* Fabrication of Transparent-Conducting-Oxide-Coated

Inverse Opals as Mesostructured Architectures for Electrocatalysis Applications: A Case Study with NiO. *ACS Appl. Mater. Interfaces* **2014**, *6*, 12290.

20. Dasgupta, N. P.; Meng, X.; Elam, J. W.; Martinson, A. B. F. Atomic Layer Deposition of Metal Sulfide Materials. *Acc. Chem. Res.* **2015**, *48*, 341.

21. Bezverkhyy, I.; Afanasiev, P.; Danot, M. Preparation of Highly Dispersed Pentlandites(M,M')$_9$S$_8$(M, M' = Fe, Co, Ni) and Their Catalytic Properties in Hydrodesulfurization. *J. Phys. Chem. B* **2004**, *108*, 7709.

22. Feng, L.-L.; Li, G.-D.; Liu, Y.; Wu, Y.; Chen, H.; Wang, Y.; Zou, Y.-C.; Wang, D.; Zou, X. Carbon-Armored Co$_9$S$_8$ Nanoparticles as All-pH Efficient and Durable H$_2$-Evolving Electrocatalysts. *ACS Appl. Mater. Interfaces* **2015**, *7*, 980.

23. Falkowski, J. M.; Surendranath, Y. Metal Chalcogenide Nanofilms: Platforms for Mechanistic Studies of Electrocatalysis. *ACS Catal.* **2015**, *5*, 3411.

24. Xu, J.; Wang, Q.; Wang, X.; Xiang, Q.; Liang, B.; Chen, D.; Shen, G. Flexible Asymmetric Supercapacitors Based upon Co$_9$S$_8$ Nanorod//Co$_3$O$_4$@RuO$_2$ Nanosheet Arrays on Carbon Cloth. *ACS Nano* **2013**, *7*, 5453.

25. Maneeprakorn, W.; Malik, M. A.; O'Brien, P. The Preparation of Cobalt Phosphide and Cobalt Chalcogenide(CoX, X = S, Se) Nanoparticles from Single Source Precursors. *J. Mater. Chem.* **2010**, *20*, 2329.

26. Yin, Y.; Erdonmez, C. K.; Cabot, A.; Hughes, S.; Alivisatos, A. P. Colloidal Synthesis of Hollow Cobalt Sulfide Nanocrystals. *Adv. Funct. Mater.* **2006**, *16*, 1389.

27. Zhang, X.; Liu, Q.; Meng, L.; Wang, H.; Bi, W.; Peng, Y.; Yao, T.; Wei, S.; Xie, Y. In-Plane Coassembly Route to Atomically Thick Inorganic−Organic Hybrid Nanosheets. *ACS Nano* **2013**, *7*, 1682.

28. Farha, O. K.; Eryazici, I.; Jeong, N. C.; Hauser, B. G.; Wilmer, C. E.; Sarjeant, A. A.; Snurr, R. Q.; Nguyen, S. T.; Yazaydn, A. Ö.; Hupp, J. T. Metal−Organic Framework Materials with Ultrahigh Surface Areas: Is the Sky the Limit? *J. Am. Chem. Soc.* **2012**, *134*, 15016.

29. Lee, J.; Farha, O. K.; Roberts, J.; Scheidt, K. A.; Nguyen, S. T.; Hupp, J. T. Metal-Organic Framework Materials as Catalysts. *Chem. Soc. Rev.* **2009**, *38*, 1450.

30. Zhao, M.; Ou, S.; Wu, C.-D. Porous Metal−Organic Frameworks for Heterogeneous Biomimetic Catalysis. *Acc. Chem. Res.* **2014**, *47*, 1199.

31. Zhang, T.; Lin, W. Metal-organic frameworks for artificial photosynthesis and photocatalysis. *Chem. Soc. Rev.* **2014**, *43*, 5982.

32. Li, J.-R.; Sculley, J.; Zhou, H.-C. Metal−Organic Frameworks for Separations. *Chem. Rev.* **2012**, *112*, 869.

33. He, Y.; Zhou, W.; Qian, G.; Chen, B. Methane Storage in Metal-Organic Frameworks. *Chem. Soc. Rev.* **2014**, *43*, 5657.

34. Suh, M. P.; Park, H. J.; Prasad, T. K.; Lim, D.-W. Hydrogen Storage in Metal−Organic Frameworks. *Chem. Rev.* **2012**, *112*, 782.

35. So, M. C.; Wiederrecht, G. P.; Mondloch, J. E.; Hupp, J. T.; Farha, O. K. Metal-Organic Framework Materials for Light-harvesting and Energy Transfer. *Chem. Commun.* **2015**, *51*, 3501.

36. Lalonde, M.; Bury, W.; Karagiaridi, O.; Brown, Z.; Hupp, J. T.; Farha, O. K. Transmetalation: Routes to Metal Exchange within Metal-Organic Frameworks. *J. Mater. Chem. A* **2013**, *1*, 5453.

37. Brozek, C. K.; Dinca, M. Cation Exchange at the Secondary Building Units of Metal-Organic Frameworks. *Chem. Soc. Rev.* **2014**, *43*, 5456.

38. Mondloch, J. E.; Bury, W.; Fairen-Jimenez, D.; Kwon, S.; DeMarco, E. J.; Weston, M. H.; Sarjeant, A. A.; Nguyen, S. T.; Stair, P. C.; Snurr, R. Q.; et al. Vapor-Phase Metalation by Atomic Layer Deposition in a Metal−Organic Framework. *J. Am. Chem. Soc.* **2013**, *135*, 10294.

39. Nguyen, H. G. T.; Schweitzer, N. M.; Chang, C.-Y.; Drake, T. L.; So, M. C.; Stair, P. C.; Farha, O. K.; Hupp, J. T.; Nguyen, S. T. Vanadium-Node-Functionalized UiO-66: A Thermally Stable MOF-Supported Catalyst for the Gas-Phase Oxidative Dehydrogenation of Cyclohexene. *ACS Catal.* **2014**, *4*, 2496.

40. Chughtai, A. H.; Ahmad, N.; Younus, H. A.; Laypkov, A.; Verpoort, F. Metal-Organic Frameworks: Versatile Heterogeneous Catalysts for Efficient Catalytic Organic Transformations. *Chem. Soc. Rev.* **2015**, 10.1039/C4CS00395K.

41. Ma, Y.; Su, H.; Kuang, X.; Li, X.; Zhang, T.; Tang, B. Heterogeneous Nano Metal−Organic Framework Fluorescence Probe for Highly Selective and Sensitive Detection of Hydrogen Sulfide in Living Cells. *Anal. Chem.* **2014**, *86*, 11459.

42. Petit, C.; Levasseur, B.; Mendoza, B.; Bandosz, T. J. Reactive Adsorption of Acidic Gases on MOF/Graphite Oxide Composites. *Microporous Mesoporous Mater.* **2012**, *154*, 107.

43. Wang, X.-L.; Fan, H.-L.; Tian, Z.; He, E.-Y.; Li, Y.; Shangguan, J. Adsorptive Removal of Sulfur Compounds Using IRMOF-3 at Ambient Temperature. *Appl. Surf. Sci.* **2014**, *289*, 107.

44. Wang, H.; Yuan, X.; Wu, Y.; Chen, X.; Leng, L.; Zeng, G. Photodeposition of Metal Sulfides on Titanium Metal-Organic Frameworks for Excellent Visible-Light-Driven Photocatalytic Cr(VI) Reduction. *RSC Adv.* **2015**, *5*, 32531.

45. Shen, L.; Luo, M.; Liu, Y.; Liang, R.; Jing, F.; Wu, L. Noble-Metal-Free MoS$_2$ Co-Catalyst Decorated UiO-66/CdS Hybrids for Efficient Photocatalytic H$_2$ Production. *Appl. Catal., B* **2015**, *166−167*, 445.

46. Yu, X.-Y.; Yu, L.; Wu, H. B.; Lou, X. W. Formation of Nickel Sulfide Nanoframes from Metal−Organic Frameworks with Enhanced Pseudocapacitive and Electrocatalytic Properties. *Angew. Chem., Int. Ed.* **2015**, *54*, 5331.

47. Abney, C. W.; Gilhula, J. C.; Lu, K.; Lin, W. Metal-Organic Framework Templated Inorganic Sorbents for Rapid and Efficient Extraction of Heavy Metals. *Adv. Mater.* **2014**, *26*, 7993.

48. Wu, R.; Wang, D. P.; Kumar, V.; Zhou, K.; Law, A. W. K.; Lee, P. S.; Lou, J.; Chen, Z. MOFs-Derived Copper Sulfides Embedded Within Porous Carbon Octahedra for Electrochemical Capacitor Applications. *Chem. Commun.* **2015**, *51*, 3109.

49. Liu, Q.; Zhang, J. A General and Controllable Synthesis of Co$_m$S$_n$(Co$_9$S$_8$, Co$_3$S$_4$, and Co$_{1-x}$S) Hierarchical Microspheres with Homogeneous Phases. *CrystEngComm* **2013**, *15*, 5087.

50. Chang, S.-H.; Lu, M.-D.; Tung, Y.-L.; Tuan, H.-Y. Gram-Scale Synthesis of Catalytic Co$_9$S$_8$ Nanocrystal Ink as a Cathode Material for Spray-Deposited, Large-Area Dye-Sensitized Solar Cells. *ACS Nano* **2013**, *7*, 9443.

51. Hamon, L.; Serre, C.; Devic, T.; Loiseau, T.; Millange, F.; Férey, G.; Weireld, G. D. Comparative Study of Hydrogen Sulfide Adsorption in the MIL-53(Al, Cr, Fe), MIL-47(V), MIL-100(Cr), and MIL-101(Cr) Metal−Organic Frameworks at Room Temperature. *J. Am. Chem. Soc.* **2009**, *131*, 8775.

52. Planas, N.; Mondloch, J. E.; Tussupbayev, S.; Borycz, J.; Gagliardi, L.; Hupp, J. T.; Farha, O. K.; Cramer, C. J. Defining the Proton Topology of the Zr$_6$-Based Metal−Organic Framework NU-1000. *J. Phys. Chem. Lett.* **2014**, *5*, 3716.

53. Gelder, E. A.; Jackson, S. D.; Lok, C. M. The Hydrogenation of Nitrobenzene to Aniline: A New Mechanism. *Chem. Commun.* **2005**, 522.

54. Park, Y. K.; Choi, S. B.; Nam, H. J.; Jung, D.-Y.; Ahn, H. C.; Choi, K.; Furukawa, H.; Kim, J. Catalytic Nickel Nanoparticles Embedded in a Mesoporous Metal-Organic Framework. *Chem. Commun.* **2010**, *46*, 3086.

55. Rasero-Almansa, A. M.; Corma, A.; Iglesias, M.; Sanchez, F. Post-functionalized Iridium-Zr-MOF as a Promising Recyclable Catalyst for the Hydrogenation of Aromatics. *Green Chem.* **2014**, *16*, 3522.

56. Attempts at conducting this catalysis with ethanol produced basic conditions inducing decomposition of the MOF scaffold. Therefore, a buffered solution is necessary as a solvent to maintain a pH in which the MOF is stable.

57. Piña, S., Jr; Cedillo, D. M.; Tamez, C.; Izquierdo, N.; Parsons, J. G.; Gutierrez, J. J. Reduction of Nitrobenzene Derivatives using Sodium Borohydride and Transition Metal Sulfides. *Tetrahedron Lett.* **2014**, *55*, 5468.